Detection of COVID-19 lesions based on computed tomography using U-Net 2.5D and GAN

José Anatiel Landim[1], Edson Carvalho[1], João Otávio Diniz[5], Alcilene Sousa[3], Daniel Luz[4], Antônio Filho[123]

[1]Electrical Engineering – Federal University of Piauí
Teresina – PI – Brazil

[2]Computer Science (Ph.D.) – Federal University of Piauí
Teresina – PI – Brazil

[3]Information Systems – Federal University of Piauí
Picos – PI – Brazil

[4]Federal Institute of Education, Science and Technology of Piauí
Picos – PI – Brazil

[5]Federal Institute of Education, Science and Technology of Maranhão
Grajaú – MA – Brazil

{anatielsantos,edsondamasceno,alcilene,antoniooseas}@ufpi.edu.br

daniel.luz@ifpi.edu.br, joao.bandeira@ifma.edu.br

Abstract. *This paper proposes a computational method for automatically detecting suspected regions of COVID-19 from CT scans. COVID-19 has spread rapidly worldwide, infecting over 462 million people and causing over 6 million deaths. There are various methods to diagnose COVID-19, including imaging. The proposed method has five stages, including image acquisition, preprocessing, lung extraction, segmentation of suspected regions using U-Net 2.5D and Pix2Pix architectures, and result validation. The method achieved promising results, with 92% Dice for lung parenchyma segmentation, 82% Dice for suspected region segmentation using U-Net, and 71% Dice using Pix2Pix. It could potentially be integrated into clinical environments as a real aid system.*

1. Introduction

On March 11, 2020, the World Health Organization declared the outbreak of the novel coronavirus as a pandemic. According to the COVID-19 Dashboard tool developed and maintained by Johns Hopkins University (JHU) [JHU 2021], COVID-19, the disease caused by the virus, has caused over 6.4 million deaths and infected more than 578 million people worldwide as of March 2022 [JHU 2021].

Vaccines for COVID-19 are currently limited to countries with financial resources, resulting in low vaccine coverage in many countries. While Brazil has shown significant decreases in pandemic numbers due to vaccination, expanding vaccine coverage worldwide is necessary to return to normality, as insufficient coverage may lead to the emergence of new virus variants [Ramos et al. 2022]. Rapid tests and RT-PCR tests are encouraged for diagnosis and fighting against COVID-19 [Bastos et al. 2020]. However,

RT-PCR tests are primarily available through private clinics and pharmacies, making it difficult for low-income populations to access them.

In addition to tests, the diagnosis of COVID-19 can be made by image exams such as chest X-ray [Freire et al. 2022] and Computerized Tomography (CT) [Costa et al. 2021]. X-ray exams are more affordable because they require more popular equipment. However, CT exams produce images with more detail, which makes the diagnosis more efficient. Since it was declared a global pandemic affected by COVID-19, scientists worldwide have been creating methods and tools that can help in the segmentation and classification of lesions caused by Severe Acute Respiratory Syndrome Coronavirus 2 (SARS-CoV-2), especially in imaging tests [Silva et al. 2023, de Sousa Filho et al. 2022, Silva et al. 2021].

This research explores classic image processing techniques in conjunction with machine learning to provide an automatic and efficient mechanism for detecting lesions caused by SARS-CoV-2 infection from CT analysis. We propose a fully automated method for detecting COVID-19 lesions from CT images using two deep learning architectures: U-Net and Pix2Pix.

Our research presents three main contributions: 1) an automatic and efficient method for lung parenchyma segmentation; 2) an automatic method for detecting regions affected by COVID-19 using U-Net 2.5D and adversary networks (Pix2Pix) to provide specialists with a more detailed clinical analysis of each detected region; and 3) a comparative study of deep learning architectures for lung region segmentation in the context of COVID-19.

The remainder of this research is divided into the following sections: Section 2 summarizes related works, Section 3 describes our methodology, Section 4 presents our qualitative and quantitative results, comparisons, and discussions of our method, and Section 5 outlines our conclusions and future work.

2. Related works

This section presents the works related to this research that segment COVID-19 lesions and lung parenchyma in CT exams. Studies on the subject have been published worldwide in search of solutions that help computer-assisted detection of COVID-19. The researches above are a sample of recent publications developed to target injuries caused by COVID-19. Table 1 presents a summary of the most relevant aspects of each work.

Table 1. Summary of related works.

Author(s)	Database	DSC (%)	Type	Architecture
Wang et al. [Wang et al. 2020]	private	80,72	automatic	COPLE-Net
Ouyang et al. [Ouyang et al. 2020]	private	-	automatic	VB-Net
Oulefki et al. [Oulefki et al. 2021]	COVID-CT	71	automatic	Limiar
Hasanzadeh et al. [Hasanzadeh et al. 2020]	private	77	automatic	U-Net
Müller et al. [Müller et al. 2020]	COVID-19 CT Ma *et al.*	76	automatic	U-Net 3D
Xu et al. [Xu et al. 2020]	COVID-19 CT JUN *et al.*	76	automatic	GAN
Fang et al. [Fang et al. 2021]	private	74	automatic	Cycle-GAN

All works analyzed, with the exception of Wang et al. [Wang et al. 2020], Ha-

sanzadeh et al. [Hasanzadeh et al. 2020] and Xu et al. [Xu et al. 2020], perform a segmentation step of the lung parenchyma. Ouyang et al. [Ouyang et al. 2020], Müller et al. [Müller et al. 2020] and Fang et al. [Fang et al. 2021] use masks of the lung region generated by the architectures proposed by them, as well as in the method proposed by this work.

Although many studies already use deep learning approaches in their conception, the proposed study intends, in more detail, to:

- Develop an automatic strategy for extracting the lung parenchyma to reduce the specialist's intervention and delimit the analysis regions for later steps;
- Carry out a study that enables the analysis of the deep learning architectures studied in this research; and,
- Investigate the effectiveness of changing architectures for analyzing the problem under study.

3. Method

In this section, we present the five steps of the proposed methodology for detecting COVID-19 lesions, which are as follows: i) Acquiring the image databases containing the CT exams; ii) Performing the pre-processing stage, which involves standardizing the input images; iii) Extracting the lungs to remove other structures that are not of interest; iv) Segmenting suspected regions affected by COVID-19 using U-Net and GAN architectures; and, v) Evaluating the results.

Figure 1 provides a summary of these steps.

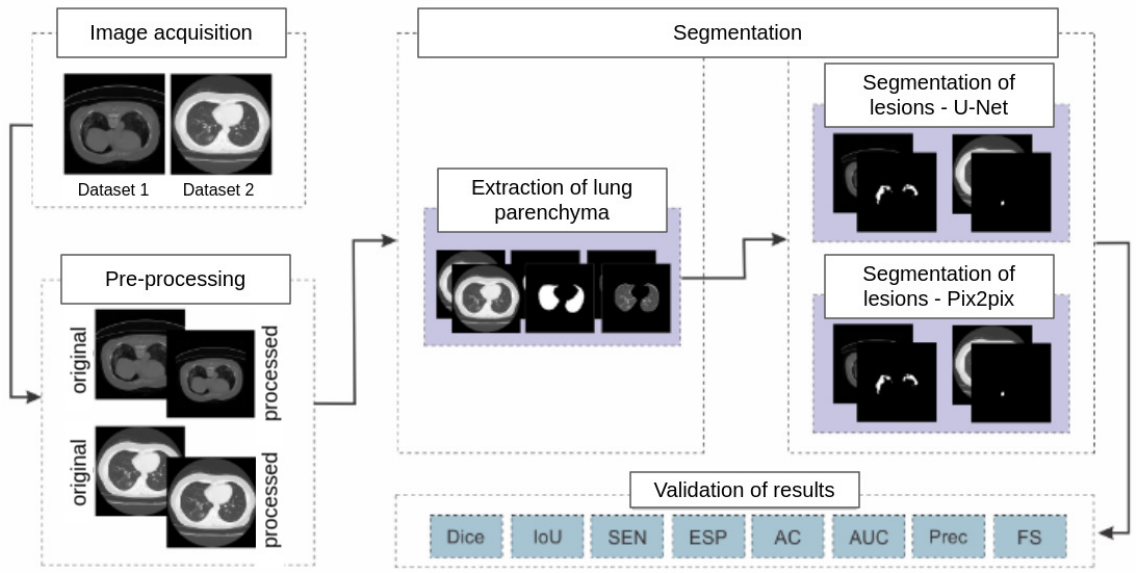

Figure 1. Proposed method.

3.1. Image acquisition

The present work uses two datasets of lung CT images obtained from public repositories in its experiments.

- Dataset 1: COVID-19 CT Lung and Infection Segmentation Dataset - this work uses exams from the image source Coronacases, composed of 10 exams and 10 lung and lesion masks. The images in this dataset have dimensions of 512x512 pixels, with up to 12bits of resolution and varying depths. In total, this dataset has 2581 images. CTs are scored by two radiologists and verified by a third radiologist [Jun et al. 2020].
- Dataset 2: COVID-19 CT Segmentation Dataset - has 9 exams, each exam has 630x630 pixels resolution, with different depths and up to 12bits of resolution. Altogether, this database contains 829 sections evaluated by a radiologist as positive or negative for COVID-19 and with lesions duly noted [MedSeg 2020].

Both datasets used have the markings of lesions and lungs. Understanding that only the region of the lung parenchyma presents the regions with lesions, we propose a sequence of steps to generate automatic masks for the parenchyma. Thus, we are considering the application of the method to bases that do not have lung markings. This process is described in Section 3.3.

3.2. Pre-processing

Each dataset has different dimensions for their exams. As our method used U-Net Architecture [Ronneberger et al. 2015] and to meet the various configurations of experiments that we performed, the images went through a process to adjust dimensions, that is, height and width. Square images avoid distortion.

Initially, we defaulted all exams to 640 x 640. For this process, we created a new volume with new dimensions (640 x 640). This volume has values 0 (zero). After that, we move the original volume to the center of the new volume. It is important to note that we have only standardized the height and width of the exam, i.e., we have not modified the depth. After, a normalization was applied to the resulting images so that they all started to have only positive pixel values, since the original images are measured in Hounsfield Units, and this one has negative and positive values.

Thus, at the end of the pre-processing stage, we obtained two datasets with dimensions of 640 x 640 pixels with images with only positive values. These new datasets were used as input to the architectures studied for the segmentation of lung parenchyma for the segmentation of COVID-19 lesions.

3.3. Lung parenchyma extraction

After standardizing the datasets, we developed a preliminary lung parenchyma extraction step. We chose to do this as it drastically reduces the search space for segmentation techniques in regions suspected of being affected by COVID-19. For lung extraction, the following steps were applied:

1. Initially, we applied the Otsu algorithm to the input image, so that the lung was separated from the other structures (Figure 2(b));
2. Next, we perform a vertical cut in the center of the image resulting from the Otsu algorithm, generating two new images (Figure 2(c));
3. For each new resulting image, the second largest region was selected, and the two extracted segments were recombined forming a new image that contains only the region of each lung, that is, the lung parenchyma (Figure 2(d));

4. After that, we apply a closing process using morphological operations to eliminate gaps present in the segmentation and edge corrections. In this step, a structuring element in the shape of a sphere was used, with radius 3 (Figure 2(e));

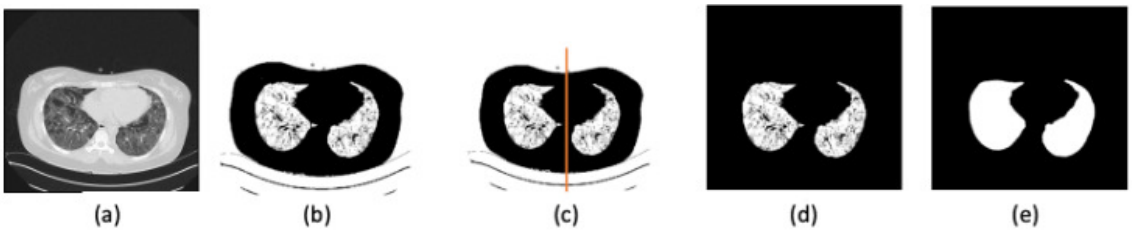

Figure 2. Sequence of steps for lung parenchyma extraction. (a) CT image; (b) Threshold with Otsu; (c) Vertical cut in the center of the image resulting from the Otsu algorithm, generating two new images; (d) Selection of the second largest region in the two images generated in the previous step; (e) Result after application of morphological operations.

The result of this processing are the images that are passed as input to the neural networks.

After generating the masks, to reduce the need for computational power, we chose to identify, from the lung masks, the largest existing bounding box between the two datasets. All images from both datasets were cut using this identified bounding box as a reference. After the end of this process, the dimensions for the two datasets became 544 x 544 pixels, smaller than the original ones for the two datasets. This reduction in dimensions contributes to reducing processing consumption and, consequently, optimizing the training time of neural networks.

3.4. Segmentation

After applying the pre-processing and lung extraction steps, this work proposes the segmentation of COVID-19 lesions. In CT, the most common lesions are ground-glass opacities, mosaic paving, consolidations, reticular opacities, subpleural lines, inverted halo sign, and pleural thickening [DE CARVALHO BRITO et al. 2021]. The proposed method explores two CNN architectures U-Net and Generative Adversarial Network (GAN).

3.4.1. U-Net

The architecture of CNN U-Net was proposed by Ronneberger et al. [Ronneberger et al. 2015] for semantic segmentation purposes. The original construction of this network consists of 23 convolutional layers interleaved by ReLU and maximum pooling operations. The architecture gets its name because it was conceived in a structure that resembles the letter U. The descent is a path of contraction, and the ascent is a path of expansion.

The hiring path follows the typical architecture of a convolutional network. It consists of the repeated application of two 3x3 convolutions (unfilled convolutions), each followed by a ReLU and a maximum 2x2 pooling operation with step 2 for downsampling.

Each step in the expansive path consists of an increase in the resolution of the feature map followed by a 2x2 convolution (up convolution) that halves the number of feature channels, a concatenation with the feature map correspondingly clipped from the contracting, and two 3x3 convolutions, followed by an activation layer ReLU [Ronneberger et al. 2015].

The model used in this work differs from the original as it uses a 2.5D approach. This approach consists of a stack of adjacent slices and producing a prediction for at least the central slice. The approach gives the network the possibility to capture 3D spatial information [Vu et al. 2020].

The U-Net is trained with slices of CT from the axial plane at a size of 544 x 544 pixels. The network takes as input a central slice and its front and back slices, i.e., three axial slices. The output of the U-Net is the segmentation mask of the central slice. The network receives an image of the CT and the mask of the specialist as input. The network train to optimize the Dice Loss function.

3.4.2. Generative Adversarial Networks

GAN is a type of architecture proposed by GOODFELLOW et al. [GOODFELLOW et al. 2014]. The principle of this network is to train two networks simultaneously. A generator *G* and a discriminator *D* where the weights of the generator and the discriminator are updated simultaneously.

The *G* network has the function of generating new data samples based on the distribution of the real training data. The *D* discriminator network estimates the probability that the sample came from the separated data for training instead of having been generated by *G* [GOODFELLOW et al. 2014].

In this research, we used the Pix2pix network, an architecture based on GAN concepts originally proposed by [Isola et al. 2017]. The Pix2Pix architecture is composed of two networks. The first is a generator G, which is built based on the U-Net conception where jump connections were added, following the general form of a U-Net. Specifically, the connections between each i layer and the $n - i$ layer are ignored, where *n* is the total number of layers. Each jump connection simply concatenates all channels in the layer with that layer $n - i$ [Isola et al. 2017]. The generating network of this work differs from the original one as it was altered by the original U-Net, described in Subsection 3.4.1.

Training together with the generator, there is too, a discriminator D, composed of a Convolutional Neural Network called PatchGAN, which consists of a Convolutional Neural Network without dense layers. This discriminator tries to classify whether each patch $N \times N$ in an image is real or fake. Run the discriminator by convolution on the image, averaging all responses to give the final output [Isola et al. 2017].

The Pix2Pix [GOODFELLOW et al. 2014], where a generator network G and a discriminator network D compete in a minimax game [GOODFELLOW et al. 2014]. The original network G has been changed to U-Net 2.5D described in Subsection 3.4.1.

Network D was kept the same as the original architecture and is composed of a Convolutional Neural Network of the PatchGAN type, described in Subsection 3.4.2.

3.4.3. Training

It is important to note that, for the network architectures to learn the behavior of COVID-19 lesions, only the CT images containing the lesions and their respective masks are given as input. Table 2 presents the configurations of the training stage for both architectures.

Table 2. Training settings

Architec.	Epochs	Opt.	Batch site	Error Func.	Learning Rate
U-Net	150	*Adam*	1	Dice loss	0.00001
Pix2pix	150	*Adam*	1	Dice loss	0.0002

At the end of each training, the best model (defined from the result of maximizing the evaluation metric Dice) was saved. This model was used in the prediction stage of the test sets exams to validate the proposed method.

3.5. Validation of results

The results were validated using the indicators: Dice coefficient (Dice), Intersection Over Union index (IoU), Sensitivity (SEN), Specificity (SPE), Accuracy (AC), Area Under the ROC Curve (AUC), Precision (Prec) and F-Score (FS). These indicators are calculated based on the prediction of the segmentation architecture and the tagging done by the expert.

4. Results and Discussion

This section presents and discusses the results obtained by the proposed method to segment the lung parenchyma and detect COVID-19 on CT scans. The experiments were performed on a machine with a 2.10 GHz Intel Xeon E5-2683 v4 processor, 128 GB of RAM, and an Ubuntu 18.04 LTS operating system.

4.1. Extraction of lung parenchyma

Before carrying out the experiments, the Datasets went through a pre-processing step (Section 3.2). Fallowing, we performed the extraction step of the lung regions. Table 3 presents the results obtained with the set of techniques proposed here.

The results observed for the segmentation of the lungs, make the proposed method a good alternative for application in image Datasets that do not have specialist masks for the lung parenchyma. It is possible to notice that the proposed method obtained an average DICE of 92%. Thus, the set of techniques for parenchyma extraction was selected to compose the proposed method. In addition to showing better results, it has a lower computational cost as it does not require a training process.

4.2. Segmentation of lesions

This section presents the results of the segmentation step of COVID-19 lesions on CT images. For this step, two architectures of CNNs previously described were used. The training settings used were described in Table 2.

Table 3. Results by examining the segmentation of the lungs with the proposed thresholding technique.

Exam	Dice	IoU	SEN	SPE	AC	AUC	Prec	FS
CT 1	0.919	0.851	0.867	0.997	0.981	0.932	0.979	0.919
CT 2	0.926	0.862	0.867	0.999	0.984	0.933	0.994	0.926
CT 3	**0.966**	**0.934**	**0.946**	**0.999**	**0.993**	**0.972**	**0.987**	**0.966**
CT 4	0.917	0.846	0.849	0.999	0.978	0.924	0.996	0.917
CT 5	0.929	0.867	0.874	0.999	0.984	0.936	0.991	0.929
CT 6	0,913	0,840	0,842	1,000	0,987	0,921	0,996	0,913
CT 7	0.918	0.849	0.852	0.999	0.979	0.926	0.995	0.918
CT 8	0.923	0.858	0.928	0.988	0.980	0.958	0.919	0.923
CT 9	0,941	0,889	0,892	1,000	0,992	0,946	0,997	0,941
Avg	**0.928**	**0.866**	**0.880**	**0.998**	**0.984**	**0.939**	**0.984**	**0.928**

To ensure that architectures can learn disease characteristics, slices without lesions are removed from training and validation sets, resulting in 1160 slices for dataset 1 and 364 slices for training and validation for dataset 2. It is important to highlight that, for the tests stage, the exams were used in their entirety, i.e., all the images contained in the patient's CT exam. For each architecture, in the detection stage of regions suspected of being affected by COVID-19, five experiments were carried out where:

1. We apply the cross-validation technique (K-fold) with K equal to 10 and 9, for the dataset 1 and dataset 2, respectively (experiment 1 and 2);
2. The training was performed with Dataset 2 and the test with Dataset 1, and vice versa (experiment 3 and 4);
3. And finally, the two datasets were mixed, and we applied K-fold with K equal to 10 (experiment 5).

Table 4 presents the average of the results obtained by experiments 1 and 2.

Table 4. Experiments 1 and 2: Results obtained for tests with the U-Net and Pix2Pix architectures.

Exp.	Dice	IoU	SEN	SPE	AC	AUC	Prec	FS
U-Net								
1	**0.73 ± 0.1**	**0.59 ± 0.1**	**0.78 ± 0.1**	**0.99 ± 0.0**	**0.99 ± 0.0**	**0.89 ± 0.0**	**0.71 ± 0.1**	**0.73 ± 0.1**
2	0.27 ± 0.2	0.18 ± 0.1	0.22 ± 0.2	0.99 ± 0.0	0.93 ± 0.0	0.61 ± 0.1	0.93 ± 0.1	0.27 ± 0.2
Pix2Pix								
1	**0.71 ± 0.1**	**0.56 ± 0.1**	**0.73 ± 0.1**	**0.99 ± 0.0**	**0.99 ± 0.0**	**0.86 ± 0.0**	**0.75 ± 0.1**	**0.71 ± 0.1**
2	0.35 ± 0.3	0.27 ± 0.3	0.49 ± 0.4	0.99 ± 0.0	0.98 ± 0.0	0.68 ± 0.3	0.60 ± 0.4	0.35 ± 0.3

Tests performed on Dataset 2 show less expressive results than those obtained in tests with Dataset 1, for two architectures. We believe that this may be due to the smaller number of image samples and the fact that this dataset contains less homogeneous exams than the dataset 1. Next, we present the results for experiments 3 and 4 (Table 5).

It is possible to notice that when the test is performed in Dataset 2, the results show a worsening compared to tests on Dataset 1. We believe that this architecture was

Table 5. Experiments 3 and 4: Results obtained for tests with the U-Net and Pix2Pix architectures.

Exp.	Training	Test	Dice	IoU	SEN	SPE	AC	AUC	Prec	FS
					U-Net					
3	Dataset 1	Dataset 2	0.14	0.09	0.11	0.99	0.92	0.55	0.33	0.14
4	**Dataset 2**	**Dataset 1**	**0.82**	**0.70**	**0.83**	**0.99**	**0.99**	**0.91**	**0.84**	**0.82**
					Pix2Pix					
3	Dataset 1	Dataset 2	0.15	0.10	0.15	0.99	0.96	0.57	0.18	0.15
4	**Dataset 2**	**Dataset 1**	**0.12**	**0.06**	**0.16**	**0.99**	**0.99**	**0.58**	**0.10**	**0.12**

not efficient in learning the characteristics of lesions in these test settings. Continuing with the flow of experiments, we have in Table 6 the results for experiment 5.

Table 6. Experiment 5: results obtained for tests with the U-Net and Pix2Pix architectures.

Exp.	Dice	IoU	SEN	SPE	AC	AUC	Prec	FS
				U-Net				
5	0.49 ± 0.2	0.37 ± 0.2	0.52 ± 0.3	0.99 ± 0.0	0.98 ± 0.0	0.76 ± 0.1	0.63 ± 0.2	0.49 ± 0.2
				Pix2Pix				
5	0.48 ± 0.3	0.37 ± 0.2	0.52 ± 0.3	0.99 ± 0.0	0.98 ± 0.0	0.76 ± 0.1	0.55 ± 0.3	0.48 ± 0.3

Experiment 5 showed lower results when compared to the other experiments. We believe that this may have occurred due to the complexity of the exams, as the CT scanners used in the acquisition of the exams are different, which causes variations in contrast, which directly influences the convergence of the model.

4.3. Discussions

The present research presented an automatic method of detecting COVID-19 using deep learning techniques to target regions suspected of being infected with the new Coronavirus. For experiments performed with U-Net, the best results were obtained in experiment 4, with a Dice of 82%. Using the Pix2pix architecture, the best results were obtained in experiment 1, with a Dice of 71%. Finally, in experiment 5, which represents a greater amount of images for training and, consequently, a greater complexity, both architectures showed acceptable results, but improvements are needed.

Table 7 presents a comparison of the proposed method with related works presented in Section 2. We know that the task of comparing results is not trivial, so the comparison made here is only quantitative without merits or demerits to other related works. We also emphasize that only a sample of the works related to this research was analyzed since this is a topic of great relevance in the last two years. The volume of published works is very large, which makes an analysis of all works unfeasible.

Table 7. Comparison with related works

Work	Dice (%)	SEN (%)	ESP (%)	Type	Exams	Slices	Lung Seg
[Wang et al. 2020]	80.72	-	-	auto.	378	76250	no
[Ouyang et al. 2020]	-	87	93	auto.	-	4982	yes
[Oulefki et al. 2021]	71	73	99	auto.	275	-	yes
[Hasanzadeh et al. 2020]	79	-	-	auto.	-	8739	no
[Müller et al. 2020]	76	73	99	auto.	20	-	yes
[Xu et al. 2020]	76.7	-	-	auto.	20	-	no
[Fang et al. 2021]	74	73	-	auto.	77	2536	yes
Our U-Net	**82**	**83**	**99**	**auto.**	**19**	**1524**	**yes**
Our GAN	71	73	99	auto.	19	1524	yes

Before comparing the results, it is important to note that some of the methods presented in related works use sets of images that are different from those used in the proposed method of this work. Additionally, not all metrics adopted in this work are present in the related works. Thus, a more accurate and faithful analysis could not be performed.

Upon analyzing Table 7, we can see that the proposed method using the U-Net architecture obtained a better Dice coefficient than the methods analyzed in related works. On the other hand, when using the Pix2pix architecture, the results presented were similar to those obtained by other works presented.

Given the advances of the proposed method, we would like to highlight the following:

- This research presents a set of techniques for lung parenchyma segmentation that are relevant and efficient, as they are simple to implement and execute compared to approaches using deep learning techniques.
- The Pix2Pix and U-Net architectures exhibit good results for the task of segmenting COVID-19 lesions, when compared with the results obtained by related works.
- The proposed method detects whether or not the patient has COVID-19 and indicates the regions suspected of being infected by COVID-19. This is extremely useful, as it provides specialists with new perspectives for analyzing the lesion.
- The architectures were applied to a series of complex and diversified experiments, evaluated through several evaluation metrics with cross-validation, ensuring that all samples have been trained and tested.

As limitations, in addition to those already known that surround methods based on deep learning, we highlight: i) The presence of false positives, specifically in the results produced by the Pix2Pix architecture; and, ii) The need for a greater amount of images so that the models can detect small lesions.

5. Conclusion

This research demonstrates that traditional techniques, such as Otsu and mathematical morphology, are efficient in extracting lung parenchyma, while the U-Net and Pix2pix

architectures can be used to identify regions suspected of being affected by COVID-19. The results obtained from experiments conducted on two public databases indicate that the proposed method can be integrated into a system to assist health professionals in real clinical settings in segmenting COVID-19 lesions and lung parenchyma on CT scans of the lungs.

In future works, we intend to apply post-processing steps to the results obtained, such as reducing false positives using morphological operations. We also plan to investigate the use of data normalization techniques, such as quantization of values, and evaluate the effectiveness of data augmentation techniques.

Referências

Bastos, M. L., Tavaziva, G., Abidi, S. K., Campbell, J. R., Haraoui, L.-P., Johnston, J. C., Lan, Z., Law, S., MacLean, E., Trajman, A., et al. (2020). Diagnostic accuracy of serological tests for covid-19: systematic review and meta-analysis. *bmj*, 370.

Costa, G., Paiva, A., Júnior, G. B., and Ferreira, M. (2021). Covid-19 automatic diagnosis with ct images using the novel transformer architecture. In *Anais do XXI Simpósio Brasileiro de Computação Aplicada à Saúde*, pages 293–301, Porto Alegre, RS, Brasil. SBC.

DE CARVALHO BRITO, V., DOS SANTOS, P. R. S., DE SALES CARVALHO, N. R., and DE CARVALHO FILHO, A. O. (2021). Covid-index: A texture-based approach to classifying lung lesions based on ct images. *Pattern Recognition*, 119:108083.

de Sousa Filho, E. L., Magno, P. G., Santos, C. J., da Silva, G. L., Diniz, J. O., and Quintanilha, D. B. (2022). Um método baseado em radiomics e mlp para diagnóstico automático de covid-19 a partir de raio-x de tórax. In *Anais da X Escola Regional de Computação do Ceará, Maranhão e Piauí*, pages 188–197. SBC.

Fang, C., Liu, Y., Liu, M., Qiu, X., Liu, Y., Li, Y., Wen, J., and Yang, Y. (2021). Unsupervised covid-19 lesion segmentation in ct using cycle consistent generative adversarial network.

Freire, N., Leão, P., Tiago, L., Gonçalves, A., Pinto, R., Santos, E., and Souto, E. (2022). Generalizability of cnn on predicting covid-19 from chest x-ray images. In *Anais do XXII Simpósio Brasileiro de Computação Aplicada à Saúde*, pages 36–47, Porto Alegre, RS, Brasil. SBC.

GOODFELLOW, I., POUGET-ABADIE, J., MIRZA, M., XU, B., WARDE-FARLEY, D., OZAIR, S., COURVILLE, A., and BENGIO, Y. (2014). Generative adversarial nets. in: Advances in neural information processing systems. page 2072–2680.

Hasanzadeh, N., Paima, S. S., Bashirgonbadi, A., Naghibi, M., and Soltanian-Zadeh, H. (2020). Segmentation of covid-19 infections on ct: Comparison of four unet-based networks. In *2020 27th National and 5th International Iranian Conference on Biomedical Engineering (ICBME)*, pages 222–225.

Isola, P., Zhu, J.-Y., Zhou, T., and Efros, A. A. (2017). Image-to-image translation with conditional adversarial networks. *2017 IEEE Conference on Computer Vision and Pattern Recognition (CVPR)*.

JHU, J. H. U. (2021). Coronavirus covid-19. Accessed Jul. 2021].

Jun, M., Cheng, G., Yixin, W., Xingle, A., Jiantao, G., Ziqi, Y., Minqing, Z., Xin, L., Xueyuan, D., Shucheng, C., Hao, W., Sen, M., Xiaoyu, Y., Ziwei, N., Chen, L., Lu, T., Yuntao, Z., Qiongjie, Z., Guoqiang, D., and Jian, H. (2020). Covid-19 ct lung and infection segmentation dataset.

MedSeg (2020). Covid-19 ct segmentation dataset.

Müller, D., Soto Rey, I., Kramer, F., and . (2020). Automated chest ct image segmentation of covid-19 lung infection based on 3d u-net.

Oulefki, A., Agaian, S., Trongtirakul, T., and Kassah Laouar, A. (2021). Automatic covid-19 lung infected region segmentation and measurement using ct-scans images. *Pattern Recognition*, 114:107747.

Ouyang, X., Huo, J., Xia, L., Shan, F., Liu, J., Mo, Z., Yan, F., Ding, Z., Yang, Q., Song, B., Shi, F., Yuan, H., Wei, Y., Cao, X., Gao, Y., Wu, D., Wang, Q., and Shen, D. (2020). Dual-sampling attention network for diagnosis of covid-19 from community acquired pneumonia. *IEEE Transactions on Medical Imaging*, 39(8):2595–2605.

Ramos, R., Ferreira, C., and Simão, A. (2022). The survival rate among unvaccinated, first dose, and second dose brazilian hospitalized and icu covid patients by age group. In *Anais do XXII Simpósio Brasileiro de Computação Aplicada à Saúde*, pages 48–59, Porto Alegre, RS, Brasil. SBC.

Ronneberger, O., Fischer, P., and Brox, T. (2015). U-net: Convolutional networks for biomedical image segmentation. *Medical Image Computing and Computer-Assisted Intervention – MICCAI 2015*, page 234–241.

Silva, L. d. J., Cortes, O., and Diniz, J. (2023). A novel ensemble cnn model for covid-19 classification in computerized tomography scans. *Results in Control and Optimization*, page 100215.

Silva, L. S., Diniz, J. O., da Silva, G. L., Silva, A. C., and Paiva, A. C. (2021). Segmentation and reconstruction of the lung in ct affected by covid-19 using deep learning and adaptive convex hull. In *17th International Symposium on Medical Information Processing and Analysis*, volume 12088, pages 56–64. SPIE.

Vu, M. H., Grimbergen, G., Nyholm, T., and Löfstedt, T. (2020). Evaluation of multislice inputs to convolutional neural networks for medical image segmentation. *Medical Physics*, 47(12):6216–6231.

Wang, G., Liu, X., Li, C., Xu, Z., Ruan, J., Zhu, H., Meng, T., Li, K., Huang, N., and Zhang, S. (2020). A noise-robust framework for automatic segmentation of covid-19 pneumonia lesions from ct images. *IEEE Transactions on Medical Imaging*, 39(8):2653–2663.

Xu, Z., Cao, Y., Jin, C., Shao, G., Liu, X., Zhou, J., Shi, H., and Feng, J. (2020). Gasnet: Weakly-supervised framework for covid-19 lesion segmentation.